Carbohydrate Polymers 89 (2012) 80–88

Contents lists available at SciVerse ScienceDirect

Carbohydrate Polymers

journal homepage: www.elsevier.com/locate/carbpol

Cellulose micro/nanofibres from *Eucalyptus* kraft pulp: Preparation and properties

G.H.D. Tonoli[a,*], E.M. Teixeira[b], A.C. Corrêa[b], J.M. Marconcini[b], L.A. Caixeta[a], M.A. Pereira-da-Silva[c,d], L.H.C. Mattoso[b]

[a] Department of Forest Science, Universidade Federal de Lavras, C.P. 3037, 37200-000 Lavras, MG, Brazil
[b] Laboratório Nacional de Nanotecnologia para o Agronegócio (LNNA), Embrapa Instrumentação (CNPDIA), Caixa Postal 741, São Carlos, SP, CEP 13560-970, Brazil
[c] Instituto de Física de São Carlos, Universidade de São Paulo, C.P. 369, 13560-970 São Carlos, SP, Brazil
[d] Centro Universitário Central Paulista - UNICEP, Brazil

ARTICLE INFO

Article history:
Received 6 December 2011
Received in revised form 18 February 2012
Accepted 20 February 2012
Available online 3 March 2012

Keywords:
Acid hydrolysis
Microfibrils
Nanofibrils
Refining
Sonication
Whiskers

ABSTRACT

There is growing interest in cellulose nanofibres from renewable sources for several industrial applications. However, there is a lack of information about one of the most abundant cellulose pulps: bleached *Eucalyptus* kraft pulp. The objective of the present work was to obtain *Eucalyptus* cellulose micro/nanofibres by three different processes, namely: refining, sonication and acid hydrolysis of the cellulose pulp. The refining was limited by the low efficiency of isolated nanofibrils, while sonication was more effective for this purpose. However, the latter process occurred at the expense of considerable damage to the cellulose structure. The whiskers obtained by acid hydrolysis resulted in nanostructures with lower diameter and length, and high crystallinity. Increasing hydrolysis reaction time led to narrower and shorter whiskers, but increased the crystallinity index. The present work contributes to the different widespread methods used for the production of micro/nanofibres for different applications.

© 2012 Elsevier Ltd. Open access under the Elsevier OA license.

1. Introduction

There is currently a growing interest in the use of more environmentally friendly materials and naturally occurring polymers, such as cellulose, for developing materials (Teixeira et al., 2010). In nature, the cellulose chains are packed in an ordered manner to form compact nanocrystals (whiskers), which are stabilized by inter and intra-molecular hydrogen bonding (Alemdar & Sain, 2008). These hydrogen bondings make the nanocrystals completely insoluble in water and in most organic solvents and lead to a material with mechanical strength only limited by the forces of adjacent atoms (Kamel, 2007). In the cell wall structures of vegetable plants, those cellulose nanocrystals (whiskers) are bonded together by amorphous holocellulose segments to form the micro/nanofibrils that constitute the individual cellulose fibres (Eichhorn et al., 2010). The term “whiskers” is used to label elongated crystalline rod-like nanofibres, whereas the designation “micro/nanofibrils” should be used to designate long flexible micro and nanofibres consisting of alternating crystalline and amorphous cellulose chains (Siqueira, Bras, & Dufresne, 2009).

Micro/nanofibres have been studied for different industrial applications: pharmaco (Villanova et al., 2011), dietary food (Okiyama, Motoki, & Yamanka, 1993), packaging and films (Bradley, Castle, & Chaudhry, in press; Siro & Plackett, 2010; Syverud, Chinga-Carrasco, Toledo, & Toledo, 2011), special papers (Nguyen & Tan, 2009; Sehaqui, Allais, Zhou, & Berglund, 2011) and especially as reinforcement in polymer matrices (Orts et al., 2005; Samir, Alloin, & Dufresne, 2005). The interrelationship between the cellulose raw material is essential for industrial applications, as well as for the processing and the quality of the final fibrillated products and also their capacity for a later industrial upscaling (Zimmermann, Bordeanu, & Strub, 2010). The geometric properties of the nanocellulose structures (shape, length and diameter) depend mainly on the extraction process and on the origin of the cellulose raw material (Ahola, Osterberg, & Laine, 2008; Siqueira, Abdillahi, Bras, & Dufresne, 2010; Siqueira et al., 2009).

Cellulose micro/nanofibres can be obtained from mechanical and chemical procedures. For the mechanical procedures the following can be mentioned: refining or high-shear homogenization process (Iwamoto, Nakagaito, & Yano, 2007; Syverud et al., 2011), microfluidization (Siqueira et al., 2009; Zimmermann et al., 2010) and sonication (Chen et al., 2011; Cheng, Wang, & Rials, 2009), which result in micro and nanofibrils. Refining and homogenizing are carried out in the presence of water, usually producing micro/nanofibrils by passing the suspension of pulp fibres through a

---

* Corresponding author. Tel.: +55 35 3829 1411; fax: +55 35 3829 1411.
E-mail addresses: gustavotonoli@dcf.ufla.br, gustavotonoli@yahoo.com.br (G.H.D. Tonoli).

0144-8617 © 2012 Elsevier Ltd. Open access under the Elsevier OA license.
doi:10.1016/j.carbpol.2012.02.052

relatively narrow gap of a disc apparatus between the rotor and the stator. In the microfluidization process the suspension is subject to high pressure to pass through a Y- or Z-type geometry interaction chamber (Zimmermann et al., 2010). Sonication is carried out in a fibre suspension in order to separate the micro/nanofibrils bundles in the fibre cell wall through cavitation (Petersson & Oksman, 2006). For the chemical procedures it can be reported: enzymatic hydrolysis with cellulases (Pääkkö et al., 2007) leading to micro and nanofibrils; and acid hydrolysis with sulphuric or hydrochloric acid (Corrêa, Teixeira, Pessan, & Mattoso, 2010) individualizing the whiskers (crystalline nanofibres). The amorphous domains around the cellulose micro/nanofibrils and between the whiskers are destroyed by acid hydrolysis under a controlled period of time and temperature, keeping the crystallites intact. The acid hydrolysis is selective in amorphous holocellulose, resulting in colloid suspensions of well-defined cellulose nanocrystals (Alemdar & Sain, 2008).

Several sources of cellulose have been used to obtain cellulose nanostructures with different morphologies and crystallinities. Examples include tunicin (Mathew & Dufresne, 2002), wheat straw (Kaushik & Singh, 2011), cotton (Teixeira et al., 2010), bacterial cellulose (Soykeabkaew, Sian, Gea, Nishino, & Peijs, 2009; Woehl et al., 2010), bamboo (Chen et al., 2011), sisal (Siqueira et al., 2009), coconut (Rosa et al., 2010), soybean (Wang & Sain, 2007), curaua (Corrêa et al., 2010), banana residues (Cherian et al., 2008), hemp (Bhatnagar & Sain, 2005) and wood (Beck-Candanedo, Roman, & Gray, 2005; Sehaqui et al., 2011). However, the potential of short fibre wood, like *Eucalyptus* species, for the production of whiskers and micro/nanofibrils deserves better investigation. In tropical regions, *Eucalyptus* is a fast growing hardwood species with good fibre qualities and relatively cheap market price (Campinhos, 1999). Among the kraft pulps produced in Brazil, bleached *Eucalyptus* kraft pulp (BEKP) is the most abundant and has increasingly become more available than other pulps in several countries. The adequate selection of starting cellulose materials can reduce energy consumption in micro/nanofibres production, a key issue for industrial upscaling. *Eucalyptus* pulp presents shorter fibres and higher hemicellulose content than *Pinus* pulp for example, which facilitates disintegration and can reduce energy input. According to Iwamoto, Abe, and Yano (2008) and Syverud et al. (2011), high contents of hemicelluloses can facilitate the release of nanofibrils during the mechanical treatment of the pulp. Therefore these advantages indicate a favourable situation for producing nanofibrils using *Eucalyptus* pulp fibres as raw material.

In the present work, micro/nanofibrils and whiskers were extracted via mechanical (refining and sonication) and chemical (acid hydrolysis) procedures from bleached *Eucalyptus* kraft pulp. The objective was to investigate the morphology, crystallinity, surface charge, and thermal stability of the *Eucalyptus* cellulose nanostructures produced via different methodologies: refining, sonication or acid hydrolysis. The influence of hydrolysis reaction time (30 min or 60 min) on the obtained properties of the whiskers was also investigated.

2. Experimental

2.1. Materials

Conventional bleached *Eucalyptus urograndis* kraft pulp, composed of approximately 99 wt.% of holocellulose (cellulose + hemicellulose) was used as starting raw-material. The cellulose fraction was composed of around 92.2 wt.% α-cellulose, 6.9 wt.% β-cellulose and 0.9 wt.% γ-cellulose, according to TAPPI T 203 cm-99 (2009) standard. Its hemicelluloses (SCAN C 4:61, 1961) and lignin (SCAN C 1:77, 1977) contents were of around 13.9 wt.% and 0.1 wt.%, respectively. Extractives (SCAN C 7:62, 1962) and ash (SCAN C 6:62, 1962) content were of around 0.1 wt.% and 0.6 wt.%, respectively.

2.2. Micro/nanofibrils production using mechanical treatment

Refining: Intact pulp (pristine fibres) was refined in a Bruno disc refiner model 2RA-12, as reported in Tonoli, Joaquim, Arsène, Bilba, and Savastano (2007) and Tonoli et al. (2011). The discs are 300 mm in diameter with 2 mm width bar, 2 mm width groove and 7.5° angle bar configuration, resulting in approximately 3 km rev^{-1} cutting edge length for the double disc refiner. The pulp was passed several times through the refiner until achieving the refining level of CSF 100 mL. The CSF test is a widely recognized standard measure of the drainage properties of pulp suspensions (Coutts & Ridikas, 1982) and it relates well to the initial drainage rate of the wet pulp pad during the de-watering process. Low freeness values (less than 300 mL) are indicative of a high degree of fibrillation and/or shortage of the fibres, leading to long drainage periods during the test. CSF values were determined after each refining level following TAPPI T 227 om-99 (1999) standard.

Sonication: The pulp fibres were processed in a knife mill (Solab) in order to obtain particle sizes lower than 0.5 mm. The milled fibres were then dried for 24 h at 50 °C before they were used. The milled fibres were swelled in demineralized water and the resulting suspension (25 g L^{-1}) was subject to 7 h sonication with a Branson 450 equipment (50% amplitude and around 80 W) in 30 min intervals in order to loosen up the micro/nanofibrils. Although the suspensions were cooled in an ice bath during sonication, an increase in local temperature should not be completely discarded. After each 30 min, a stable micro/nanofibril suspension was obtained at the suspension supernatant, which was centrifuged in order to separate the micro/nanofibrils.

2.3. Nanofibre production using chemical treatment

Acid hydrolysis: Whiskers (crystalline nanofibres) were extracted from the milled fibres by acid hydrolysis with sulphuric acid 60% (v/v) at around 45 °C. Two reaction times were tested (30 min and 60 min) in acid under mechanical stirring. After each conditioning time the resulting suspension was centrifuged (10,000 rpm for 10 min) for acid elimination. Next, the material was neutralized via dialysis under continuous water flux.

2.4. Characterization of the micro/nanofibres

2.4.1. Fibre and micro/nanofibre morphology

Optical microscopy (OM): An Olympus BX51 (Japan) optical microscope was used for the initial investigation of the morphologies of the pristine fibres, milled fibres and agglomerates of micro/nanofibres. Whisker films were produced after drying the suspension in petri dishes at 30 °C for 48 h. These films were then redispersed in distilled water in order to visualize the agglomerates in the optical microscope (OM). The suspensions were stained with a drop of ethanol–safranin–astrablue in order to increase the contrast between the phases. Measurements were performed with image analyses software (Image-ProPlus 5-1.0.20, Media Cybermetrics, 2004). Only the typical images of each fibre condition are presented in the present work.

Atomic force microscopy (AFM): Multimode Nanoscope IIIa atomic force microscope Digital Instrument at tapping-mode (TM-AFM) was used to study the fibre surface topography and the micro/nanofibre morphology, the data was acquired simultaneously by means of height and phase imaging. Silicon cantilever with a spring constant of around 70 N m^{-1} (Digital Instruments, 1996) and a scan area of 3 μm × 3 μm were used and all the images were measured in atmospheric (air) environment (temperature ca. 25 °C and relative humidity between 50 and 65%). The samples were evaluated as individualized fibres. Fibres and micro/nanofibres were dispersed at around 0.03 g L^{-1} concentration and some drops were deposited onto a glass microscope slide. Before AFM imaging, the samples were dried (60 °C for 12 h) on the glass slides and bonded onto the sample stubs. The images were processed from raw data using the software NanoScope III version 5.12b43 (2002) to perform the dimensional measurements of the fibres and micro/nanofibres. Approximately ten measurements were taken for each condition, but only representative images of the samples are shown in the present work.

Scanning transmission electron microscopy (STEM): Nanofibres were also assessed in a transmission electron microscope (TEM) Tecnai^{TM} G2 F20, in bright and dark field scanning transmission electron microscopy (STEM) mode. The samples were prepared with the diluted nanofibre neutral suspension, adding uranil acetate as corant and submitting the resulting suspension to sonication (Branson 450) for 2 min. A suspension drop was deposited to a copper grid with Formvar film (400 mesh – Ted Pella), and maintained in the dessicator for 24 h for drying before it was used in STEM. The average diameter and length of the micro/nanofibrils and whiskers were determined by using digital image analyses (Image-ProPlus 5-1.0.20, Media Cybermetrics, 2004) of the STEM micrographs and only the representative images of each condition are presented in this work. A minimum of 100 measurements was used to determine the diameter and length distribution of the micro/nanofibres.

2.4.2. *Crystallinity of the fibres/micro/nanofibres*

The X-ray diffraction (XRD) patterns were measured for the milled fibres and their respective micro/nanofibres with an X-ray diffractometer (Shimadzu XRD-6000), using CuKα radiation at 30 kV and 30 mA. Scattered radiation was detected in the range of $2\theta = 5$–40°, at a scan rate of 1° min^{-1}. The crystallinity index (CI) was estimated from the heights of the (0 0 2) peak ($2\theta \sim 22.5^\circ$) and the minimum intensity between the (0 0 2) and (1 0 1) peaks (2θ between 18° and 22°), by means of Buschle-Diller–Zeronian equation (Buschle-Diller & Zeronian, 1992).

2.4.3. *Zeta-potential and elemental analysis*

Potential charges on the surface of fibres and micro/nanofibres in pure water were measured with a Malvern 3000 Zetasizer. Cellulose fibres and micro/nanofibres suspensions (0.06 wt.%), previously sonified for 5 min, were prepared and analyzed to determine their zeta-potential.

The dry-basis components of the materials were investigated by using ultimate analysis technique with an elemental analyzer. Elemental analysis was performed mainly to determine the total sulphur content before and after the extraction of nanofibres with sulphuric acid. It was carried out using a Vario Micro Cube CHNS-O elemental analyzer.

2.4.4. *Thermogravimetry*

Dried fibres and nanofibres were subject to thermogravimetric analysis (TG) in a TA Q500 thermal analyzer (TA Instruments, New Castle, DE, USA). The samples with around 12 mg were heated in a Pt crucible from 25 to 600 °C in air flowing at 60 mL min^{-1}. The heating rate was 10 °C min^{-1}. The critical weight loss temperatures (T_{onset}) were obtained from the onset points of the TG curves, and this was represented by the intersection of the extrapoling line, at the beginning of the thermal event, with the tangent of the curve in the thermal event.

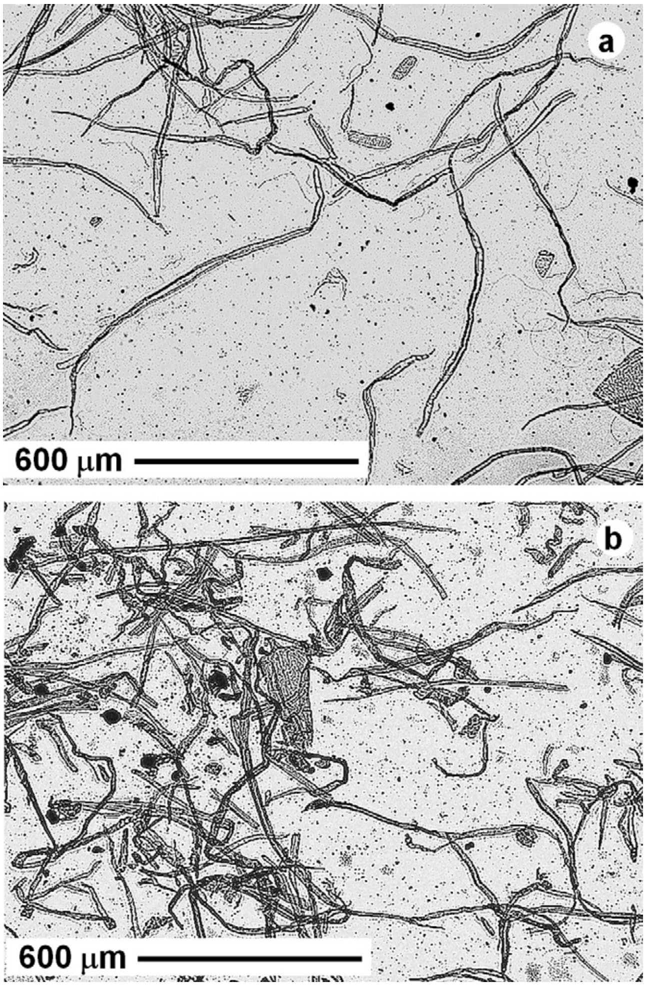

Fig. 1. Typical optical microscopy (25×) images of the (a) pristine pulp fibres and (b) after milling.

3. Results and discussion

3.1. *Morphological characteristics*

Fig. 1 shows the images of the pristine fibres and after milling. It is observed that milling decreased significantly the average length of the fibres but increased their swelling capacity because it made their extremities more reactive for the extraction of the nanofibres via sonication (cavitation) and via acid hydrolysis. The pristine fibres (Fig. 1a) presented average diameter and length of 17 ± 4 μm and 701 ± 295 μm, respectively. The milled fibres (Fig. 1b) had an average diameter and length of around 16 ± 4 μm and 271 ± 141 μm, respectively.

SEM observation showed the microfibrillation of the fibres after refining (Fig. 2-left), which was related to the decrease in freeness or drainability values (CSF) ranging from 600 mL to 130 mL. The microfibrils were pulled out from the fibre cell wall during mechanical treatment (Fig. 2b). In order to explain what occurs in the fibre cell wall with refining, Fig. 2(right) exhibits the typical fibrillar structures on the surface of the *Eucalyptus* pristine fibres. The micro/nanofibrils in these images are on average around 30 nm in diameter for both refined and unrefined fibres. The micro/nanofibrils are more exposed in the refined fibre (Fig. 2b-left) than the micro/nanofibrils in the pristine unrefined fibre (Fig. 2a-left). This is a consequence of the mechanical treatment (shearing action) on the fibre surface during refining (Tonoli et al., 2007).

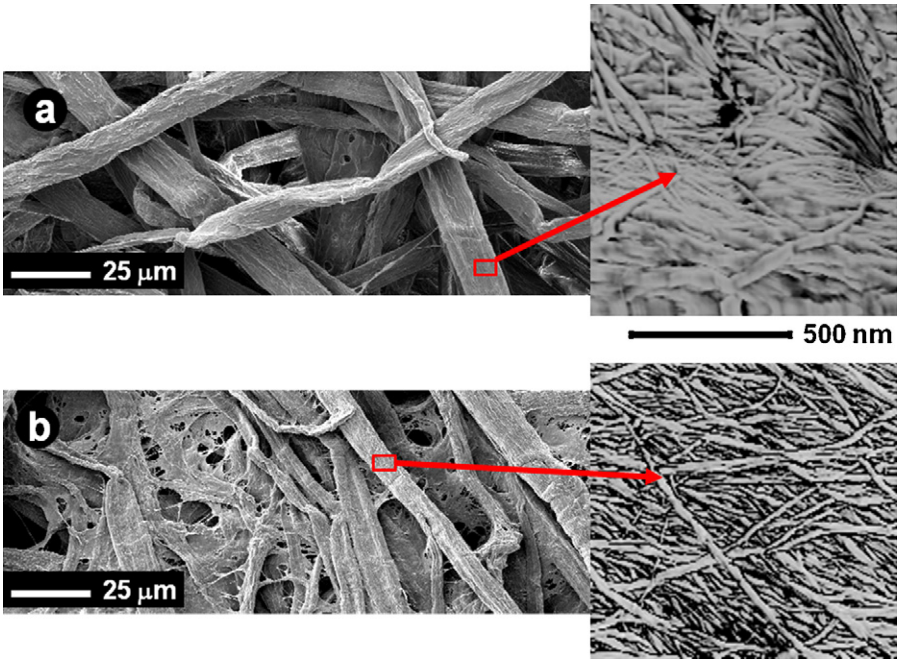

Fig. 2. Typical SEM micrographs (left) and AFM phase images (right) of (a) pristine unrefined (CSF 600 mL) and (b) refined (CSF 130 mL) *Eucalyptus* bleached fibres.

Fig. 3 depicts the microscopy images (left: OM, centre: AFM and right: STEM) of the refined fibres and micro/nanofibres obtained via sonication and acid hydrolysis.

As previously shown in Fig. 2b, refining the pristine fibres resulted in the fibrillation of the fibre surface (arrows in Fig. 3a-left) due to the pull out of micro/nanofibrils during the friction/shearing forces of refining. The diameter and length distribution of the micro/nanofibres is presented in Fig. 4. The nanofibril content obtained by refining (Fig. 3a) was very low, only few microfibrous elements of diameter size lower than 100 nm (Fig. 4a) and length lower than 500 nm (Fig. 4b). This observation shows that the refining process should be associated to a pre-treatment or is used as a pre-treatment in order to improve nanofibril yield from conventional cellulose kraft pulp. Souza et al. (2010) submitted curaua fibres to a previous mechanical defibrillation followed by refining, resulting in higher nanofibre contents with an average diameter of 50 nm.

Fig. 3b shows the micro/nanofibrils obtained via cavitation during sonication of the milled fibre suspensions. A higher magnification of the surface of unrefined fibres (Fig. 2a-right) showed a micro/nanofibrils bundle that is similar to the one observed by AFM and STEM on the supernatant fraction after sonication (Fig. 3b-centre and b-right). It was observed that cavitation was effective to open the structure of the milled fibres, releasing the micro/nanofibrils that form the fibre cell wall (arrow in Fig. 3b-left). The diameter of the micro/nanofibrils generally varied between 20 and 50 nm, and the length ranged between 200 nm and 2.5 μm, resulting in aspect ratios (L/D) between 10 and 50. The dimensions of these micro/nanofibrils are similar to that obtained via sonication by Cheng et al. (2009). The sediment fraction was formed by macroscopic fibres with diameter ranging between 2 and 20 μm and length exceeding 500 μm.

The yield of whiskers (crystalline nanofibres) via hydrolysis was determined by weight difference. As expected, the yield, in relation to the starting milled fibres, decreased from 65% to 61% with the hydrolysis time increase (from 30 min to 60 min), as a consequence of the disintegration of amorphous cellulose and degradation of the crystalline domains during hydrolysis (Bondeson, Mathew, & Oksman, 2006). Fig. 3c-left and d-left exhibits the OM images of the agglomeration of whiskers obtained with 30 min and 60 min of acid hydrolysis, respectively. Fig. 3c-left and d-left shows some pieces of fibres that were not completely hydrolyzed.

The AFM micrographs of whiskers obtained by acid hydrolysis are shown in Fig. 3c-centre and d-centre. Whiskers achieved with 30 min hydrolysis (Fig. 3c-centre) have 60% of their well individualized crystals lower than 30 nm in diameter, while 80% of the nanocrystals obtained with 60 min hydrolysis (Fig. 3d-centre) were lower than 30 nm in diameter (Fig. 4a). Fig. 3c-right and d-right shows the whiskers (well individualized crystals) visualized by STEM. However, the measurements obtained by STEM agree with the behaviour found by AFM, where 65% of the whiskers from 30 min hydrolysis (Fig. 3c) had a length lower than 200 nm, while 70% obtained from 60 min hydrolysis (Fig. 3d) had a length lower than 200 nm. Therefore, as also observed for black spruce cellulose by Beck-Candanedo et al. (2005), the continuity of acid hydrolysis during higher reaction times continues the degradation/pelling-off of the glucose chains that constitute the whiskers, decreasing their dimensions. These length dimensions agree with that obtained by Beck-Candanedo et al. (2005) for *Eucalyptus* whiskers; however the average diameter of the whiskers presented by those authors was lower than the average diameter presented here (5 nm vs. 15 nm).

The average diameter and length of the whiskers after 30 min hydrolysis were 15 ± 6 nm and 175 ± 38 nm, respectively, giving rise to an aspect ratio (L/D) of around 12. The average diameter and length of the whiskers after 60 min hydrolysis were 11 ± 4 nm and 142 ± 49 nm, respectively, giving rise to an aspect ratio (L/D) of around 14. This is similar to cellulose whiskers extracted from cotton ($L/D \sim 10$) (Dong, Revol, & Gray, 1998), ramie ($L/D \sim 12$) (Menezes, Siqueira, Curvelo, & Dufresne, 2009), common lawn grass (L/D from 12 to 20) (Pandey, Chu, Kim, Lee, & Ahn, 2009), curaua (L/D from 13 to 17) (Corrêa et al., 2010), but lower than the values found by Beck-Candanedo et al. (2005), which extracted whiskers from *Eucalyptus* ($L/D \sim 29$) and black spruce (L/D from 21 to 28), and lower than that extracted from coconut husk ($L/D \sim 40$) (Rosa et al., 2010), sisal ($L/D \sim 43$) (Siqueira et al., 2009) and "capim dourado" (Golden grass) ($L/D \sim 67$) (Siqueira et al., 2010).

The better utilization of the reinforcing potential of individual fibres may consists of using nano-sized cellulosic material as

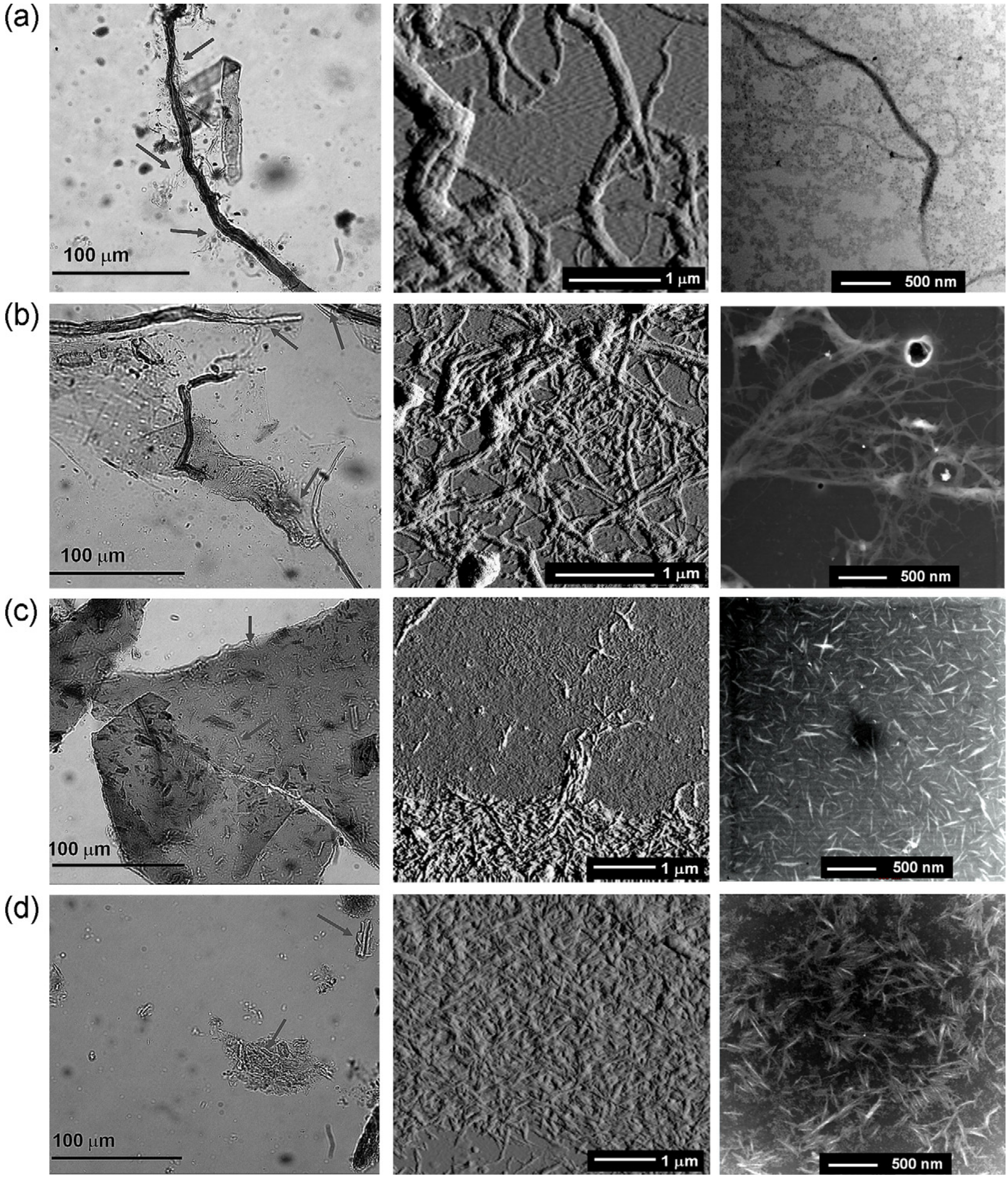

Fig. 3. Typical optical microscopy – OM (100×) images (left), AFM phase images (centre) and STEM images (right) of the micro and nanofibres obtained from the different process: (a) arrows show the microfibrils pulled out after refining; (b) arrows show the microfibres obtained by sonication; (c) and (d) whiskers after 30 min and 60 min hydrolysis respectively.

reinforcement instead of micro-sized fibres to prepare nanocomposite with high strength, stiffness, and transparency (Besbes, Vilar, & Boufi, 2011). In fact, for nanofibrils and whiskers, the reinforcing potential is controlled by the ability of the nanofiller to form a percolated network held by strong hydrogen bonding interactions that contribute to increasing the stiffness as well as the strengthening potential into polymeric composites (Malainine, Mahrouz, & Dufresne, 2005; Pullawan, Wilkinson, & Eichhorn, 2010). Siqueira et al. (2009) confirmed in their study that the reinforcing effect on the composites depends on the micro/nanofibre entanglements, which are consequence of their morphology (diameter and length). According to those authors (Siqueira et al., 2009), the use of micro/nanofibrils instead of whiskers allows obtaining not only stiffer but more brittle nanocomposite films.

3.2. Crystallinity changes

Fig. 5 shows the X-ray diffractograms (XRD) of the fibres, micro/nanofibrils and whiskers. These patterns are typical of semicrystalline materials with an amorphous broad hump and

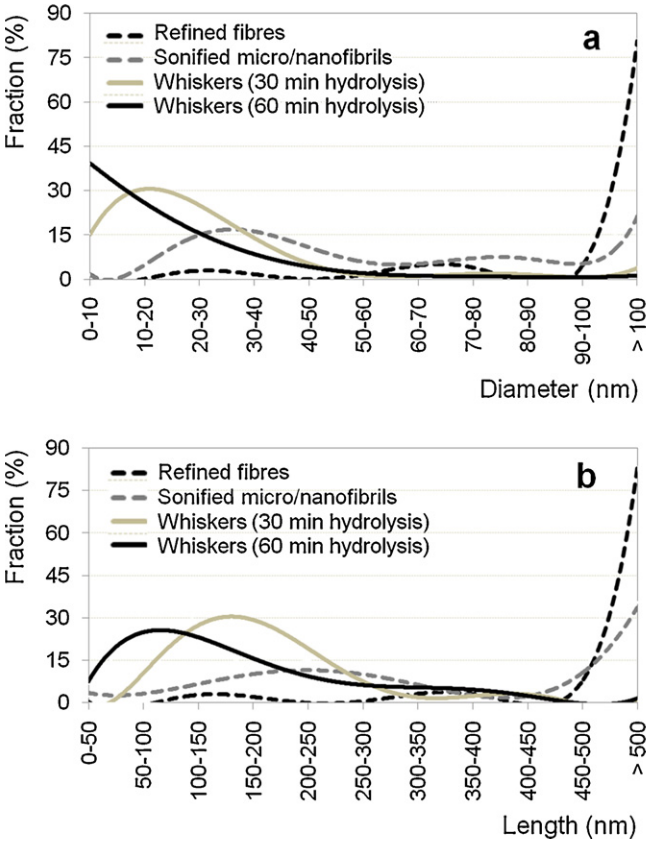

Fig. 4. Diameter (a) and length (b) distribution of the micro/nanofibres obtained via refining, sonication and acid hydrolysis.

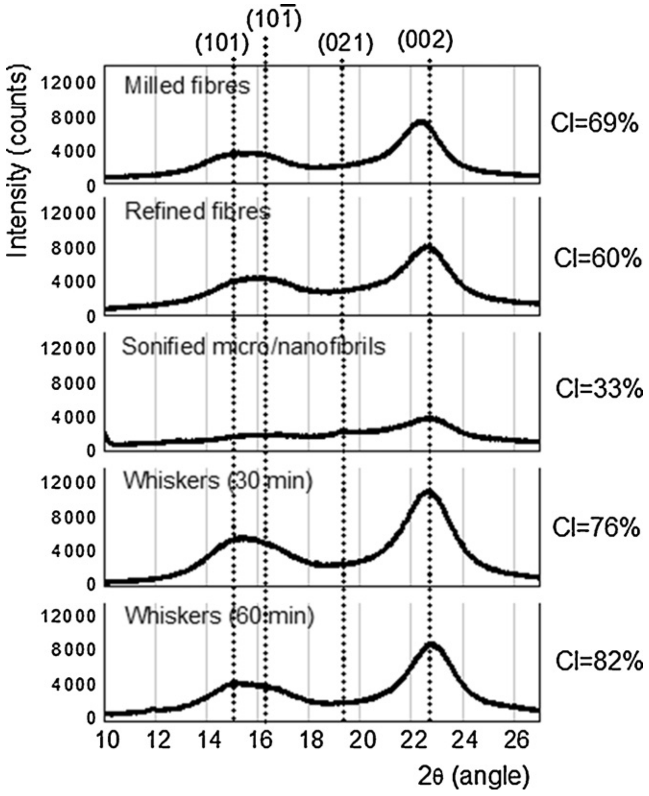

Fig. 5. X-ray diffractograms (XRD) and the calculated crystallinity index (CI) of the fibres, micro/nanofibrils and whiskers in the different conditions.

crystalline peaks. All fibre samples exhibit a sharp high peak at $2\theta = 22.6^\circ$, which is assigned to the (0 0 2) lattice plane of cellulose I. XRD showed minor variation in the position of the cellulose I (0 0 2) reflection for milled fibres (Fig. 5), attributed to differences in sample geometry. The two overlapped weaker diffractions at $2\theta = 14.8^\circ$ and $2\theta = 16.3^\circ$ are assigned to the (1 0 1) and (1 0 $\bar{1}$) lattice planes of cellulose I (Besbes et al., 2011; Klemm, Heublein, Fink, & Bohn, 2005). Cellulose I is a structure performed by repeating β-(1 → 4)-D-glucopyranose units, building blocks of parallel glucan chains (Pääkkö et al., 2007). Compared with the pristine fibres, the nanofibre samples did not exhibit any evolution in their polymorphic type. From these data, the crystallinity index (CI in Fig. 5) was determined as presented in Section 2.

The decrease in the crystallinity index (CI) was observed for the refined fibres. After refining, it changes from CI = 69% for milled fibres to CI = 60%, which is the result of the damage the crystallites underwent during the high shearing action suffered by the fibres in the refining treatment. Sonified micro/nanofibrils presented a drastic drop in the crystallinity index (CI = 33%) due to the action of hydrodynamic forces associated with ultrasound during the isolation of nanofibrils by sonication. The strong mechanical oscillating power performed by sonication acts by separating the glucose chains in the cellulose nanocrystals, despite the fact that no glucose solubilization is expected. Chen et al. (2011) also reported some damage to the crystalline domain of nanofibres when ultrasonic treatment was applied.

Whiskers presented a higher crystallinity index (CI) than the others due to the disruption of amorphous holocellulose surrounding and embedding the cellulose crystallites formed by well organized glucose chains (Wang, Sain, & Oksman, 2007). The increase in crystallinity with hydrolysis time was also due to the continuous removal of amorphous domains with time (Chen et al., 2011). Whiskers with high crystallinity could be more effective in providing better reinforcement to the flexible polymeric matrices because of the high modulus of elasticity of the crystal domain (Eichhorn et al., 2010). Moreover, less crystalline domains are less stiff than nanocrystals, which can perform improved ductility in stiff polymeric matrices (Wang & Sain, 2006).

3.3. *Zeta-potential*

Table 1 depicts the average values and standard deviations of zeta-potential and sulphur content for milled fibres, micro/nanofibrils and whiskers. Higher values of zeta-potential indicate higher capacity of dispersion in water, while low values indicate low dispersion stability. For sonified micro/nanofibrils the dispersion is prejudiced. The dispersion difference between micro/nanofibrils and whiskers could be related to the possibility of entanglement (due to the higher length) and the presence of residual pectins at the surface of micro/nanofibrils (Siqueira et al., 2009). Pectins and hemicelluloses are not expected to be present at the surface of the whiskers because they are eliminated during the hydrolysis treatment. Pectins also can act as a binder between cellulose micro/nanofibrils, improving the load transference mechanism to the reinforcement in the composites (Dufresne, Cavaille, & Vignon, 1997).

As expected, the whiskers presented higher sulphur content (Table 1), which increases the surface charges in the nanofibres obtained by hydrolysis with sulphuric acid (Podsiadlo et al., 2005). The increase in hydrolysis time from 30 to 60 min increased the sulphur content, but decreased the zeta-potential of the whiskers. Dong et al. (1998) reported the decrease of length and surface charge with higher hydrolysis time in cotton and sulphuric acid. The zeta-potential values found for the *Eucalyptus* whiskers in the present work are similar to that reported by Corrêa et al. (2010) and Teixeira et al. (2010) for curaua and cotton whiskers, respectively.

Table 1
Average values and standard deviations of the zeta-potential of the fibres and micro/nanofibres from different conditions.

	Milled fibres	Refined fibres	Sonified micro/nanofibrils	Whiskers (30 min)	Whiskers (60 min)
Zeta-potential (mV)	−49.8 ± 3.1	–	−19.1 ± 0.4	−34.2 ± 3.2	−24.5 ± 0.1
Sulphur content (wt.%)	0.03 ± 0.01	0.01 ± 0.01	0.15 ± 0.04	0.49 ± 0.03	0.98 ± 0.08

Actually, whiskers prepared with sulphuric acid present negative charge surface, while those prepared with hydrochloric acid are not charged (Samir et al., 2005). The high stability of whisker suspensions is due to the electrostatic repulsion between the negative sulphate groups on the surface of the whiskers (Dufresne, 2006; Lima & Borsali, 2004).

3.4. Thermal analysis

Acid hydrolysis decreased the onset degradation temperature (T_{onset}) of the whiskers (Fig. 6), as also observed elsewhere by Teixeira et al. (2010) for cotton whiskers. Thermal analysis (TG) of the fibres, micro/nanofibrils and whiskers showed two thermal degradation stages. The first stage occurred at temperatures of 150–350 °C, with weight loss of around 70% for fibres and 40% for micro/nanofibrils and whiskers. The second stage is the thermal degradation between 350 and 525 °C. No thermal event was observed at temperatures higher than 550 °C (Fig. 6).

As observed in the DTG curves (Fig. 7), decomposition of the starting fibre and micro/nanofibres occurred essentially in two stages, indicating the presence of different components that decompose at different temperatures. For the starting milled fibres, refined fibres and sonified micro/nanofibrils, the dominant thermogravimetric (DTG) peak was observed at around 310 °C, responsible for the maximum rate of weight loss of hemicelluloses (normally in the range of 225–325 °C), residual lignin (in the range of 250–500 °C) and cellulose (in the range of 305–375 °C) as reported by Prins, Ptasinski, and Janssen (2006), while the decomposition of the solid residues in the starting and refined fibres occurred at around 440 °C.

No dominant thermogravimetric (DTG) peak was observed for micro/nanofibrils and whiskers. Whiskers (from 30 min and 60 min hydrolysis) presented lower onset decomposition temperatures and began to degrade at around 180 °C and 230 °C (Fig. 7). This is because the thermal degradation of cellulose crystals containing sulphate groups occurs at lower temperatures (Roman & Winter, 2004; Wang, Ding, & Cheng, 2007). According to Figs. 6 and 7, thermal degradation occurred first in whiskers produced with 60 min hydrolysis, which present high sulphate groups (Table 1), leading to dehydration reactions that release water and catalyze the cellulose degradation reactions (Corrêa et al., 2010). The replacement of OH groups with sulphate groups decreases the activation energy of cellulose chain degradation (Wang et al., 2007b). This observation may limit the use of whiskers produced with 60 min hydrolysis for polymer matrices that do not require high processing temperatures (e.g. above 180 °C). The last peak of decomposition (at around 470 °C) is related to the decomposition of the solid residues.

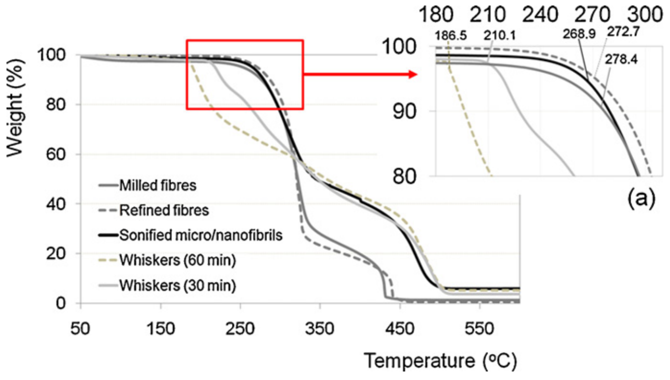

Fig. 6. TG thermograms of the fibres, micro/nanofibrils and whiskers in the different conditions: (a) detail of the onset degradation temperature (T_{onset}).

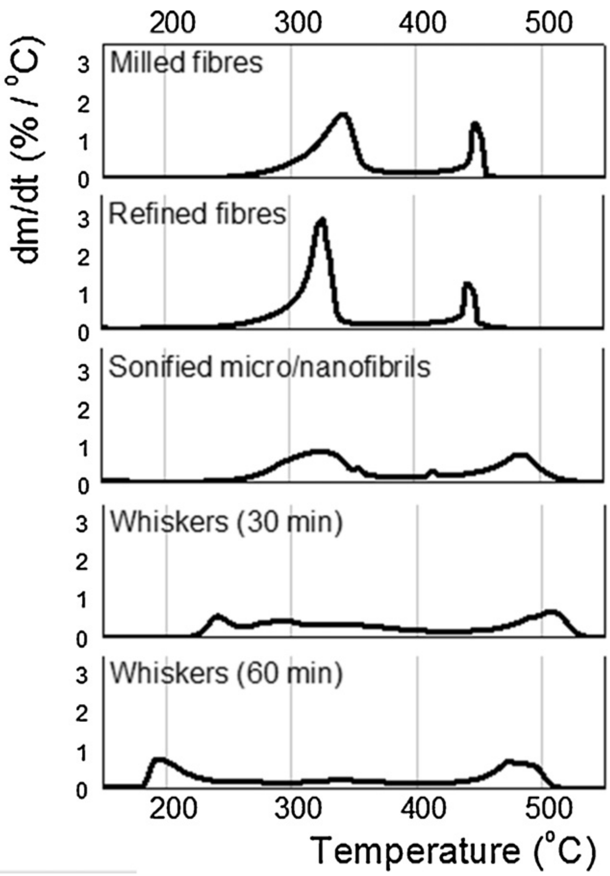

Fig. 7. DTG curves of the fibres and micro/nanofibres in the different conditions.

4. Conclusion

It was shown that *Eucalyptus* cellulose micro/nanofibres can be isolated using mechanical (refining and sonication) and chemical (acid hydrolysis) processes. The content of nanofibrils obtained by refining was very low, presenting only some microfibrous elements with diameters lower than 100 nm. The action of hydrodynamic forces associated with ultrasound during sonication was effective to open the structure of the milled fibres, releasing the micro/nanofibrils that form the fibre cell wall. However, the strong mechanical oscillating power performed by the present sonication conditions greatly diminished the crystallinity of the micro/nanofibrils, resulting in substantial damage to the cellulose structure. Sonified micro/nanofibres presented similar diameters and higher lengths than the whiskers. Longer hydrolysis reaction time (60 min) leads to narrower and shorter cellulose whiskers, with higher crystallinity index but lower thermal stability than whiskers produced with 30 min of hydrolysis. The effect of sulphur content on the surface charge of the whiskers was less clear.

The surface charge of the whiskers is highly sensitive to heat, and an increase in temperature can catalyze cellulose degradation when the sulphate groups are on the surface of the cellulose crystals, leading to thermal degradation at lower temperatures than the micro/nanofibrils obtained mechanically. The present work contributes to the widespread use of different methods for the production of *Eucalyptus* micro/nanofibres, which originate micro/nanofibres with distinct morphological and structural characteristics that can be used to engineer polymeric composites for different applications.

Acknowledgements

Financial support for this research was provided by the following Brazilian agencies: Fundação de Amparo à Pesquisa do Estado de São Paulo - FAPESP (Process N. 2009/10734-6 and 2007/50863-4), Fundação de Amparo à Pesquisa do Estado de Minas Gerais - FAPEMIG, Financiadora de Estudos e Projetos/Ministério da Ciência e Tecnologia - FINEP/MCT, Coordenação de Aperfeiçoamento de Pessoal de Nível Superior - CAPES, Empresa Brasileira de Pesquisa Agropecuária - EMBRAPA and Conselho Nacional de Desenvolvimento Científico e Tecnológico - CNPq.

References

Ahola, S., Osterberg, M., & Laine, J. (2008). Cellulose nanofibrils – Adsorption with poly(amideamine) epichlorohydrin studied by QCM-D and application as a paper strength additive. *Cellulose*, *15*, 303–314.

Alemdar, A., & Sain, M. (2008). Isolation and characterization of nanofibers from agricultural residues – Wheat straw and soy hulls. *Bioresource Technology*, *99*, 1664–2167.

Beck-Candanedo, S., Roman, M., & Gray, D. G. (2005). Effect of reaction conditions on the properties and behavior of wood cellulose nanocrystal suspensions. *Biomacromolecules*, *6*, 1048–1054.

Besbes, I., Vilar, M. R., & Boufi, S. (2011). Nanofibrillated cellulose from TEMPO-oxidized eucalyptus fibres: Effect of the carboxyl content. *Carbohydrate Polymers*, *84*, 975–983.

Bhatnagar, A., & Sain, M. (2005). Processing of cellulose nanofibers-reinforced composites. *Journal of Reinforced Plastics and Composites*, *24*, 1259–1268.

Bondeson, D., Mathew, A., & Oksman, K. (2006). Optimization of the isolation of nanocrystals from microcrystalline cellulose by acid hydrolysis. *Cellulose*, *13*, 171–180.

Bradley, E. L., Castle, L., & Chaudhry, Q. Applications of nanomaterials in food packaging with a consideration of opportunities for developing countries. *Trends in Food Science & Technology*, in press.

Buschle-Diller, G., & Zeronian, S. H. (1992). Enhancing the reactivity and strength of cotton fibers. *Journal of Applied Polymer Science*, *45*, 967–979.

Campinhos, E., Jr. (1999). Sustainable plantations of high-yield Eucalyptus trees for production of fiber: The Aracruz case. *New Forests*, *17*, 129–143.

Chen, W., Yu, H., Liu, Y., Hai, Y., Zhang, M., & Chen, P. (2011). Isolation and characterization of cellulose nanofibers from four plant cellulose fibers using a chemical-ultrasonic process. *Cellulose*, *18*, 433–442.

Cheng, Q., Wang, S., & Rials, T. G. (2009). Poly(vinyl alcohol) nanocomposites reinforced with cellulose fibrils isolated by high intensity ultrasonication. *Composites Part A: Applied Science and Manufacturing*, *40*, 218–224.

Cherian, B. M., Pothan, L. A., Nguyen-Chung, T., Mennig, G., Kottaisamy, M., & Thomas, S. (2008). A novel method for the synthesis of cellulose nanofibril whiskers from banana fibers and characterization. *Journal of Agricultural Food Chemistry*, *56*, 5617–5627.

Corrêa, A. C., Teixeira, E. M., Pessan, L. A., & Mattoso, L. H. C. (2010). Cellulose nanofibers from curaua fibers. *Cellulose*, *17*, 1183–1192.

Coutts, R. S. P., & Ridikas, V. (1982). Refined wood fibre-cement products. *Appita*, *35*, 395–400.

Digital Instruments. (1996). *Instruction manual for multimode scanning probe microscope – Version 4.22*. Santa Barbara, pp. 11–29

Dong, X. M., Revol, J. F., & Gray, D. G. (1998). Effect of microcrystallite preparation conditions on the formation of colloid crystals of cellulose. *Cellulose*, *5*, 19–32.

Dufresne, A. (2006). Comparing the mechanical properties of high performances polymers nanocomposites from biological sources. *Journal of Nanoscience and Nanotechnology*, *3*, 322–330.

Dufresne, A., Cavaille, J. Y., & Vignon, M. R. (1997). Mechanical behavior of sheets prepared from sugar beet cellulose microfibrils. *Journal of Applied Polymer Science*, *64*, 1185–1194.

Eichhorn, S. J., Dufresne, A., Aranguren, M., Marcovich, N. E., Capadona, J. R., Rowan, S. J., et al. (2010). Review: Current international research into cellulose nanofibres and nanocomposites. *Materials Science*, *45*, 1–33.

Iwamoto, S., Abe, K., & Yano, H. (2008). The effect of hemicelluloses on wood pulp nanofibrillation and nanofiber network characteristics. *Biomacromolecules*, *9*, 1022–1026.

Iwamoto, S., Nakagaito, A. N., & Yano, H. (2007). Nano-fibrillation of pulp fibers for the processing of transparent nanocomposites. *Applied Physics A*, *89*, 461–466.

Kamel, S. (2007). Nanotechnology and its applications in lignocellulosic composites, a mini review. *Express Polymer Letters*, *1*, 546–575.

Kaushik, A., & Singh, M. (2011). Isolation and characterization of cellulose nanofibrils from wheat straw using steam explosion coupled with high shear homogenization. *Carbohydrate Research*, *346*, 76–85.

Klemm, D., Heublein, B., Fink, H. P., & Bohn, A. (2005). Cellulose: Fascinating biopolymer and sustainable raw material. *Angewandte Chemie International Edition*, *44*, 2–37.

Lima, M. M. S., & Borsali, R. (2004). Rodlike cellulose microcrystals: Structure, properties, and applications. *Macromolecular Rapid Communications*, *25*, 771–787.

Malainine, M. E., Mahrouz, M., & Dufresne, A. (2005). Thermoplastic nanocomposites based on cellulose microfibrils from *Opuntia ficus-indica* parenchyma cell. *Composites Science and Technology*, *65*, 1520–1526.

Mathew, A. P., & Dufresne, A. (2002). Morphological investigations of nanocomposites from sorbitol elasticized starch and tunicin whiskers. *Biomacromolecules*, *3*, 609–617.

Menezes, A. P., Siqueira, G., Curvelo, A. A. S., & Dufresne, A. (2009). Extrusion and characterization of functionalized cellulose whiskers reinforced polyethylene nanocomposites. *Polymer*, *50*, 4552–4563.

Nguyen, X. T., & Tan, Z. (2009). Surface treatment with texturized microcrystalline cellulose microfibrils for improved paper and paper board. *Patent United States Patent 7,497,924*.

Okiyama, A., Motoki, M., & Yamanka, S. (1993). Bacterial cellulose IV. Application to processed foods. *Food Hydrocolloids*, *6*, 503–511.

Orts, W. J., Shey, J., Imam, S. H., Glenn, G. M., Guttman, M. E., & Revol, J. F. (2005). Application of cellulose microfibrils in polymer nanocomposites. *Journal of Polymers and the Environment*, *13*, 301–306.

Pääkkö, M., Ankerfors, M., Kosonen, H., Nykänen, A., Ahola, S., Österbeg, M., et al. (2007). Enzymatic hydrolysis combined with mechanical shearing and high-pressure homogenization for nanoscale cellulose fibrils and strong gels. *Biomacromolecules*, *8*, 1934–1941.

Pandey, J. K., Chu, W. S., Kim, C. S., Lee, C. S., & Ahn, S. H. (2009). Bio-nano reinforcement of environmentally degradable polymer matrix by cellulose whiskers from Grass. *Composites Part B: Engineering*, *40*, 676–680.

Petersson, L., & Oksman, K. (2006). Preparation and properties of biopolymer-based nanocomposite films using microcrystalline cellulose. In K. Oksman, & M. Sain (Eds.), *Cellulose nanocomposites: Processing, characterization and properties*. Washington, DC: American Chemical Society. ACS Symposium Series, 938, 256 pp.

Podsiadlo, P., Choi, S.-Y., Shim, B., Lee, J., Cuddihy, M., & Kotov, N. A. (2005). Molecularly engineered nanocomposites: Layer-by-layer assembly of cellulose nanocrystals. *Biomacromolecules*, *6*, 2914–2918.

Prins, M. J., Ptasinski, K. J., & Janssen, F. J. J. G. (2006). Torrefaction of wood. Part 1. Weight loss kinetics. *Journal of Analytical and Applied Pyrolysis*, *77*, 28–34.

Pullawan, T., Wilkinson, A. N., & Eichhorn, S. J. (2010). Discrimination of matrix–fibre interactions in all-cellulose nanocomposites. *Composites Science and Technology*, *70*, 2325–2330.

Roman, M., & Winter, W. T. (2004). Effect of sulfate groups from sulfuric acid hydrolysis on the thermal degradation behavior of bacterial cellulose. *Biomacromolecules*, *5*, 1671–1677.

Rosa, M. F., Medeiros, E. S., Malmonge, J. A., Gregorski, K. S., Wood, D. F., Mattoso, L. H. C., et al. (2010). Cellulose nanowhiskers from coconut husk fibers: Effect of preparation conditions on their thermal and morphological behavior. *Carbohydrate Polymers*, *81*, 82–93.

Samir, M. A. S. A., Alloin, F., & Dufresne, A. (2005). Review of recent research into cellulosic whiskers, their properties and their application in nanocomposite field. *Biomacromolecules*, *6*, 612–626.

SCAN Standard. (1977) C 1:77, Kappa number.

SCAN standard. (1961) C 4:61, Pentosans in pulp.

SCAN standard. (1962) C 6:62, Ash in wood and pulp.

SCAN Standard. (1962) C 7:62, Dichloromethane extract of pulp.

Sehaqui, H., Allais, M., Zhou, Q., & Berglund, L. A. (2011). Wood cellulose biocomposites with fibrous structures at micro- and nanoscale. *Composites Science and Technology*, *71*, 382–387.

Siqueira, G., Abdillahi, H., Bras, J., & Dufresne, A. (2010). High reinforcing capability cellulose nanocrystals extracted from *Syngonanthus nitens* (Capim Dourado). *Cellulose*, *17*, 289–298.

Siqueira, G., Bras, J., & Dufresne, A. (2009). Cellulose whiskers versus microfibrils: Influence of the nature of the nanoparticle and its surface functionalization on the thermal and mechanical properties of nanocomposites. *Biomacromolecules*, *10*, 425–432.

Siro, I., & Plackett, D. (2010). Microfibrillated cellulose and new nanocomposite materials: A review. *Cellulose*, *17*, 459–494.

Souza, S. F., Leão, A. L., Cai, J. H., Wu, C., Sain, M., & Cherian, B. M. (2010). Nanocellulose from curaua fibers and their nanocomposites. *Molecular Crystals and Liquid Crystals*, *522*, 42[342]–52[352].

Soykeabkaew, N., Sian, C., Gea, S., Nishino, T., & Peijs, T. (2009). All-cellulose nanocomposites by surface selective dissolution of bacterial cellulose. *Cellulose*, *16*, 435–444.

Syverud, K., Chinga-Carrasco, G., Toledo, J., & Toledo, P. G. (2011). A comparative study of *Eucalyptus* and *Pinus radiata* pulp fibres as raw materials for production of cellulose nanofibrils. *Carbohydrate Polymers*, *84*, 1033–1038.

TAPPI Useful Method. (1999). *T 227 om-99: Freeness of pulp (Canadian standard method)*. (Atlanta, GA, USA).

TAPPI Useful Method. (2009). *T 203cm-99: Alpha-, beta- and gamma-cellulose in pulp*. (Atlanta, GA, USA).

Teixeira, E. M., Corrêa, A. C., Manzoli, A., Leite, F. L., Oliveira, C. R., & Mattoso, L. H. C. (2010). Cellulose nanofibers from white and naturally colored cotton fibers. *Cellulose*, *17*, 595–606.

Tonoli, G. H. D., Joaquim, A. P., Arsène, M.-A., Bilba, K., & Savastano, H., Jr. (2007). Performance and durability of cement based composites reinforced with refined sisal pulp. *Materials and Manufacturing Processes*, *22*, 149–156.

Tonoli, G. H. D., Savastano, H., Jr., Santos, S. F., Dias, C. M. R., John, V. M., & Lahr, F. A. R. (2011). Hybrid reinforcement of sisal and polypropylene fibres in cement based composites. *Journal of Materials in Civil Engineering*, *23*, 177–187.

Villanova, J. C. O., Ayres, E., Carvalho, S. M., Patrício, P. S., Pereira, F. V., & Oréfice, R. L. (2011). Pharmaceutical acrylic beads obtained by suspension polymerization containing cellulose nanowhiskers. *European Journal of Pharmaceutical Sciences*, *42*, 406–415.

Wang, N., Ding, E., & Cheng, R. (2007). Thermal degradation behaviours of spherical cellulose nanocrystals with sulfate groups. *Polymer*, *48*, 3486–3493.

Wang, B., & Sain, M. (2006). Dispersion of soybean stock-based nanofiber in plastic matrix. In K. Oksman, & M. Sain (Eds.), *Cellulose nanocomposites: Processing, characterization and properties*. Washington, DC: American Chemical Society. ACS Symposium Series, 938, 256 pp.

Wang, B., & Sain, M. (2007). Isolation of nanofibers from soybean source and their reinforcing capability on synthetic polymers. *Composites Science and Technology*, *67*, 2521–2527.

Wang, B., Sain, M., & Oksman, K. (2007). Study of structural morphology of hemp fiber from the micro to the nanoscale. *Applied Composite Materials*, *14*, 89–103.

Woehl, M. A., Canestraro, C. D., Mikowski, A., Sierakowski, M. R., Ramos, L. P., & Wypych, F. (2010). Bionanocomposites of thermoplastic starch reinforced with bacterial cellulose nanofibres: Effect of enzymatic treatment on mechanical properties. *Carbohydrate Polymers*, *80*, 866–873.

Zimmermann, T., Bordeanu, N., & Strub, E. (2010). Properties of nanofibrillated cellulose from different raw materials and its reinforcement potential. *Carbohydrate Polymers*, *79*, 1086–1093.